Bioactive Materials 9 (2022) 157–167

Contents lists available at ScienceDirect

Bioactive Materials

journal homepage: www.sciencedirect.com/journal/bioactive-materials

Photoacoustic and magnetic resonance imaging-based gene and photothermal therapy using mesoporous nanoagents

Hao Huang [a,b,1], Guotao Yuan [b,1], Ying Xu [a], Yuan Gao [c], Qiulian Mao [a], Yin Zhang [b], Lu Bai [b], Weijie Li [b], Anqing Wu [a], Wentao Hu [a,*], Yue Pan [b,**], Guangming Zhou [a,***]

[a] State Key Laboratory of Radiation Medicine and Protection, School of Radiation Medicine and Protection, Collaborative Innovation Center of Radiological Medicine of Jiangsu Higher Education Institutions, Soochow University, Suzhou, 215123, China
[b] Guangdong Provincial Key Laboratory of Malignant Tumor Epigenetics and Gene Regulation, Guangdong-Hong Kong Joint Laboratory for RNA Medicine, Medical Research Center, Sun Yat-Sen Memorial Hospital, Sun Yat-Sen University, Guangzhou, 510120, PR China
[c] Department of Nutrition and Food Hygiene, Soochow University of Public Health, Suzhou, 215123, China

ARTICLE INFO

Keywords:
Gene therapy (GT)
Porous iron oxide nanoagents (PIONs)
Photothermal therapy (PTT)
Long noncoding RNA CRYBG3

ABSTRACT

The integration of photothermal therapy (PTT) with gene therapy (GT) in a single nanoscale platform demonstrates great potential in cancer therapy. Porous iron oxide nanoagents (PIONs) are widely used as magnetic nanoagents in the drug delivery field and also serve as a photothermal nanoagent for photothermal therapy. However, the therapeutic efficacy of PIONs-mediated GT has not been studied. The long noncoding RNA (lncRNA) CRYBG3 (LNC CRYBG3), a lncRNA induced by heavy ion irradiation in lung cancer cells, has been reported to directly bind to globular actin (G-actin) and cause degradation of cytoskeleton and blocking of cytokinesis, thus indicating its potential for use in GT by simulating the effect of heavy ion irradiation and functioning as an antitumor drug. In the present study, we investigated the possibility of combining PIONs-mediated PTT and LNC CRYBG3-mediated GT to destroy non-small cell lung cancer (NSCLC) cells both *in vitro* and *in vivo*. The combination therapy showed a high cancer cell killing efficacy, and the cure rate was better than that achieved using PTT or GT alone. Moreover, as a type of magnetic nanoagent, PIONs can be used for magnetic resonance imaging (MRI) and photoacoustic imaging (PAI) both *in vitro* and *in vivo*. These findings indicate that the new combination therapy has high potential for cancer treatment.

1. Introduction

Nanoagents are a type of nanomaterials that are widely used in biological research to deliver drugs [1–4], and one of such nanoagents is porous iron oxide nanoagents (PIONs). PIONs are used as a vehicle because of their specific magnetic and photothermal properties [5–10]. Near infrared (NIR) laser-induced photothermal therapy (PTT), a minimally invasive therapy, has received increasing attention in recent years because of its specific lesion destruction feature and favorable biosafety [11]. As a NIR laser-absorbing nanoagent, PIONs can kill cancer cells by transforming NIR laser energy into heat energy and deliver drugs into tumor cells under the guidance of magnetic resonance imaging (MRI). PTT can also induce an anti-tumor immune response, which is beneficial in clinical treatment [12–15]. However, during the process of PTT, the heat energy not only kills cancer cells but also induces side effects on the adjacent normal tissues [9,16,17]. According to a recent study, the combination of PTT and other adjuvant therapies can increase treatment efficacy and decrease the side effects [18–24]. Because PIONs are magnetic nanomaterials, they have the potential to be guided to tumor tissues by a magnetic field and can be used for MRI [25–27], which is very important and useful in clinical treatment. (see Scheme 1)

Gene therapy (GT) is a new type of cancer therapy. In the past decade, clinicians have used biomolecules such as siRNA/shRNA to modulate gene expression [28–32]. However, recently, molecular

Peer review under responsibility of KeAi Communications Co., Ltd.
* Corresponding author.
** Corresponding author.
*** Corresponding author.
E-mail addresses: wthu@suda.edu.cn (W. Hu), panyue@mail.sysu.edu.cn (Y. Pan), gmzhou@suda.edu.cn (G. Zhou).
[1] These authors contributed equally to this work.

https://doi.org/10.1016/j.bioactmat.2021.07.025
Received 28 May 2021; Received in revised form 5 July 2021; Accepted 21 July 2021
Available online 28 July 2021

targeted therapy has been facing challenges such as increasing drug resistance due to the development of compensatory mechanisms of the targeted pathways in cancer cells [33,34]. In our previous studies, the long noncoding RNA (lncRNA) CRYBG3 (LNC CRYBG3), a lncRNA induced by heavy ion irradiation in lung cancer cells, was shown to depolymerize the actin cytoskeleton, induce cell death, inhibit tumor progression, and decrease the invasiveness of lung cancer cells [35,36]. The actin cytoskeleton is essential for cell proliferation and growth, especially for cell division by maintaining the spatial structure of cells and helping in molecule transport in the cytoplasm and cell junction formation. Actin is the main protein of the microfilament cytoskeleton and a key factor of contractile ring formation during the middle stage of metamitosis. These findings indicated that LNC CRYBG3 may be a potential therapeutic target for GT.

Base on the above, we investigated the possibility of combining PIONs-mediated PTT and LNC CRYBG3-mediated GT to destroy non-small cell lung cancer cells (A549). For this purpose, plasmid pcDNA3.1-LNC CRYBG3 was constructed and delivered to A549 cells through PIONs to overexpress LNC CRYBG3. A549 cells were then exposed to NIR laser. The results showed that PIONs could effectively carry pcDNA3.1-LNC CRYBG3 into cancer cells and that LNC CRYBG3 was successfully overexpressed in lung cancer cells. In the combinational therapy, on one side, the heat generated by PIONs after NIR irradiation can increase the release efficiency of pcDNA3.1-LNC CRYBG3 into tumor tissues. Moreover, the heat generated during the photothermal conversion can ablate tumor tissues noninvasively by heating the tissues locally above 42 °C, while keeping the surrounding tissues from hyperpyrexia [37–40]. On the other side, in response to heavy ion irradiation, LNC CRYBG3 can overexpress in tumor cells to degrade the actin cytoskeleton and cause cell apoptosis [35,36], which simulates the tumor-killing effect of heavy ion irradiation but does not cause side effects of radiotherapy. Photothermal ablation and cytotoxicity of LNC CRYBG3 functioned together and showed synergistic cancer inhibitory effect.

2. Experimental section

2.1. Materials

All reagents involved in our experiment were used directly [11]. Polyacrylamide (PAM), ferric chloride, urea, trisodium citrate dihydrate, absolute ethanol, monobasic potassium phosphate, disodium phosphate dodecahydrate, and dimethyl sulfoxide (DMSO) were of analytically pure grade. All of the above reagents were purchased from Shanghai Chemical Reagents Co., Ltd (Shanghai, China). Plasmid overexpressing LNC CRYBG3 (pcDNA3.1-LNC CRYBG3) was designed and synthesized by Shanghai Sangon Corporation (Shanghai, China). Cell Counting Kit-8 (CCK-8) was purchased from Beyotime Biotechnology Corporation (Shanghai, China). The Lipofectamine™ 3000 (Lipo3000) Transfection Reagent (Invitrogen, Thermo Fisher Scientific, NC, USA) was used for plasmid transfection. All aqueous solutions were prepared using 18.2 MΩ•cm purified water obtained from a Milli-Q water purification system (Millipore, Bedford, MA, USA).

2.2. Preparation of PIONs

PIONs were prepared according to a modified protocol [11]. Specifically, 2.6 g ferric chloride, 3.6 g urea, and 9.4 g sodium citrate were mixed with 380 mL of deionized water and stirred with a glass rod for 30 min. Subsequently, 2.0 g of PAM was slowly added under vigorous stirring, and the stirring was continued until PAM was completely dissolved. Transferring 190 mL of the resultant solution to a 200 mL autoclave lined with Teflon and kept at 200 °C for 12 h. The resultant product was then collected by centrifugation and washed several times with absolute ethanol and ultrapure water alternately.

2.3. Photothermal properity test of PIONs

The photothermal conversion efficiency (η) of PIONs was calculated according to Roper's method and the following formulation [41].

$$\eta = [hS(T_{max} - T_{surr}) - Q_{dis}]/[I(1 - 10^{-A808})] \quad (1)$$

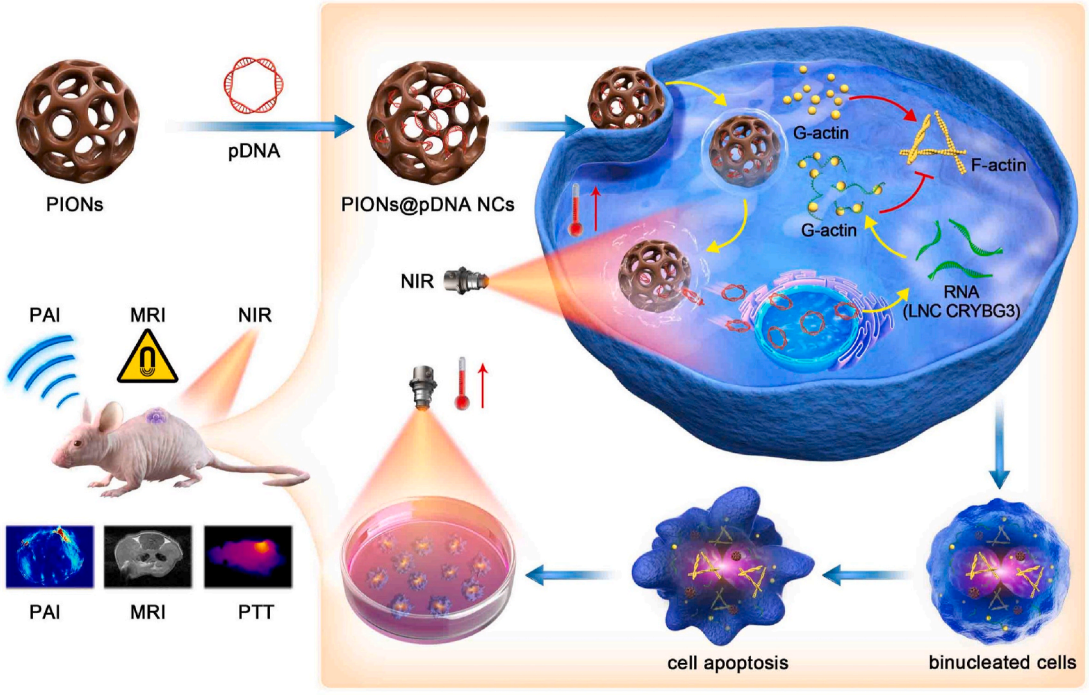

Scheme 1. Schematic illustration of using PIONs loaded with pcDNA3.1-LNC CRYBG3 nano-complexes (PIONs@pDNA NCs) as a photoporation nanoplatform for photothermal therapy and gene therapy.

In formula (1), h is the thermal conductivity coefficient; S is the laser irradiation area; T_{max} is the maximum equilibrium temperature (42 °C); T_{surr} is the surrounding ambient temperature (25.1 °C); Q_{dis} is the thermal dissipation value of the solvent and container (quartz cell or Eppendorf (EP) tube) (148.8 mW); I represents the laser irradiation current (1.35 A); and A808 represents the absorbance of PIONs (200 μg/mL) at a wavelength of 808 nm (0.9174). The value of hS is derived from Equation (2):

$$hS = m_i c_{H2O}/\tau_s \quad (2)$$

In formula (2), the m_i represents the mass of PIONs (1.0014 mg); c_{H2O} is the heat capacity of deionized water (4.2 J/g); and τ_s is the thermal conductivity of the system. The value of τ_s is calculated according to Equations (3) and (4) as follows:

$$t = -\tau_s \ln(\theta) \quad (3)$$

$$\theta = (T - T_{surr})/(T_{max} - T_{surr}) \quad (4)$$

2.4. Cell culture

Non-small cell lung cancer cells (A549) and normal human bronchial epithelium cells (BEAS-2B) were purchased from American Type Culture Collection (Rockville, MD, USA). A549 cells were cultured in Roswell Park Memorial Institute (RPMI) 1640 medium (Gibco, Grand Island, NY, USA) supplemented with 10 % fetal bovine serum (FBS), 1 % penicillin sodium, and 100 μg/mL streptomycin. BEAS-2B cells were cultured in Dulbecco's Modified Eagle's Medium (DMEM) (Gibco) containing 10 % FBS, 1 % penicillin sodium and 100 μg/mL streptomycin. All the cell lines were incubated in a 37 °C incubator (Thermo Fisher Scientific, NC, USA) with 5 % (v/v) CO_2. Trypsin was used to detach cells from the culture dish when they have grown to appropriate confluence. Then cells were collected by centrifugation at 1000 rpm for 5 min, and resuspended in a fresh culture medium to end the digestion before further treatment.

2.5. Plasmid load and release

First, 5 mg of PIONs was dissolved in double-distilled water (ddH_2O) at the concentration of 2.5 mg/mL and ultrasonically dispersed for approximately 10 min. The pcDNA3.1-LNC CRYBG3 was then dissolved in 2 mL of the prepared PIONs aqueous solution, and the mixture was then placed in a constant temperature incubator at 37 °C for 24 h to reach equilibrium. Subsequently, the PIONs@pDNA NCs were collected with a magnet and washed twice with phosphate-buffered saline (PBS) to remove free pDNA. All the supernatants were collected, and the amount of pDNA in the supernatant was measured by UV–vis–NIR spectroscopy with an absorption peak at 480 nm. The difference between the added amount of pDNA and the remaining amount was calculated to determine the amount of pDNA loaded into the PIONs.

To determine the pDNA loading capacity (PLC), 1.0 mg PIONs@pDNA NCs was dispersed in 1.0 mL neutral PBS (pH 7.4). The supernatant was collected with a magnet at different time points under the condition of slight shaking. We also conducted laser-triggered release studies of plasmids. The PIONs@pDNA NCs dispersed in PBS (pH 5.0) were treated with intermittent lasers; the continuous irradiation time was 10 min, and the laser power density was 1 W/cm^2. The same method was used to determine the pDNA loading efficiency (PLE) of PIONs. PLC and PLE were calculated using the following formulas (1) and (2):

$$\text{PLC (wt. \%)} = \text{weight of loaded pDNA / total weight of PIONs@pDNA NCs} \times 100\% \quad (1)$$

$$\text{PLE (\%)} = \text{weight of loaded pDNA / weight of added pDNA} \times 100\% \quad (2)$$

2.6. Cytotoxicity assay

Cytotoxicity of PIONs was evaluated by the CCK-8 assay. Briefly, A549 cells were seeded onto a 96-well plate at the density of 1×10^4 cells per well and grew overnight. Subsequently, the old culture medium was removed and a fresh culture medium with different concentrations (25, 50, 100, 150, 200, and 250 μg/mL) of PIONs was added into the plate. Then the cells were incubated at 37 °C for 24 h. The CCK-8 reagent was then directly added to the medium. After 2 h incubation at 37 °C, the absorbance was recorded at 450 nm by a multifunctional microplate reader (BioTek Instruments, VT, USA).

2.7. qRT-PCR

The total RNA was extracted from cells using TRIzol reagent (Invitrogen, CA, USA). The PrimeScript RT Reagent Kit (Takara Shuzo Co., Kusatsu, Shiga, Japan) was used to reverse-transcribe total mRNA, and SYBR Green qPCR Master Mix (Life Technologies, Grand Island, NY, USA) was used for cDNA amplification. Real-time PCR was performed with a Vii7A system (Life Technologies) using the following program: initiation at 95 °C for 10 min, 45 thermal cycles each at 95 °C for 15 s and at 60 °C for 20 s, and final extension at 72 °C for 15 min. All the data were analyzed with the C(t) value comparison method. The expression level of LNC CRYBG3 was normalized to that of glyceraldehyde-3-phosphate dehydrogenase (GAPDH). The primer sets used in the experiment are listed in Table S1.

2.8. Western blot

A549 cells were seeded in 60 mm cell culture dishes and treated with NIR, PIONs or PIONs@pDNA as mentioned in above experiment. The cells' protein was collected using RIPA lysing buffer (Beyotime, Shanghai, China) and determined by using BCA Protein Assay Kit (Beyotime, Shanghai, China). The 10 % SDS-PAGE gels were used to separate the proteins and 0.22 μm polyvinylidene fluoride (PVDF) membrane (Millipore, Bedford, MA, USA) was used for protein transferration. F/G-actin Western blot was performed by using the G-actin/F-actin In Vivo Assay Kit (Cytoskeleton, Inc. DENVER, USA). The jasplakinolide (Cayman Chemical Compan, Czech Republic Cayman Europe, Estonia) is a macrocyclic peptide come from sponge Jaspis johnstoni, which can induce actin to polymerize into microfilaments (F-actin) [42].

2.9. Immunofluorescence

Immunofluorescence staining was used to measure the cytoskeleton change. A549 cells were seeded in a 6-well plate with 13 mm glass slides at the density of 1×10^5 cells per well and grew overnight. Subsequently, the old culture medium was removed and a fresh culture medium with PIONs, PIONs@pDNA, or pDNA (Lipo3000) was added to the plate respectively. Then the cells were exposed to NIR (1 W/cm^2) for 10 min and incubated at 37 °C for 24 h. After incubation, the slides with cells were fixed with 4 % paraformaldehyde. The nucleus was stained with DAPI and cytoskeleton protein was stained with phalloidin. The laser scanning confocal microscope was used to take images. The percentage of binucleated cells was determined according to binucleated cells' number in every 200 cells. Phalloidin was purchased from FCMACS Biotech Co. Ltd (Nanjing, China) and used for cytoskeleton staining.

2.10. Flow cytometry

Flow Cytometry assay was used to detect the apoptosis rates of cells. A549 cells were seeded in a 6-well plate at the density of 2×10^5 cells per well and grew overnight. Subsequently, the old culture medium was removed and the fresh culture medium with PIONs, PIONs@pDNA, or pDNA (Lipo3000) was added to the plate respectively. Then cells were

exposed to NIR (1 W/cm^2) for 10 min and incubated at 37 °C for 24 h. After incubation, all cells were collected and centrifuged at 1000 rpm for 5 min. Then the supernatant was discarded and cells were resuspended with binding buffer. The apoptosis rates of cells were analyzed by flow cytometry using an Annexin V-Alexa Fluor® 647/PI/Apoptosis detection kit (cat. no. FMSAV647-100, FCMACS Biotech Co. Ltd., Nanjing, China) according to the manufacturer's protocol.

2.11. Lysosomal escape test of PIONs

A549 cells were seeded onto 35 mm glass bottom dishes at a density of 8 × 10^4 cells/dish and cultured at 37 °C until the cell confluency reached 50–60 %. Then replace the old culture medium with 1 mL of fresh medium containing Cy5.5-labeled PIONs (PIONs-Cy5.5). The concentration of PIONs was set as 200 μg/mL. Nuclei and lysosomes were stained with DAPI (1 μg/mL) and LysoTracker Red (1 μM) dyes respectively and incubated at 37 °C incubator for 30 min. Intracellular distribution of PIONs-Cy5.5 was analyzed with laser scanning confocal microscope (Olympus FV1200, Tokyo, Japan). LysoTracter Red probe was purched form KeyGEN Biotech (Nanjing, China).

2.12. Animal experiments

Male BALB/c nude mice (6–8 weeks, 18–22 g) were purchased from Shanghai SLAC Laboratory Animal Co., Ltd. and were raised in specific pathogen-free (SPF) animal rooms. The animal experimental protocols were reviewed and approved by the Institutional Animal Care and Use Committee, Soochow University.

The PIONs were dispersed in an agarose gel and solidified at room temperature. Different concentrations of PIONs were tested by a photoacoustic (PA) imaging machine and then uniformly dispersed. For *in vivo* imaging, the tumor was injected with PBS (25 μL) or PIONs solution (25 μL, 1 mg/mL) and immediately imaged with the PA scan machine. The same approach was used to test the MR imaging property of PIONs.

A549 cells were seeded onto several 100-mm culture dishes and then harvested. Next, 5 × 10^6 cells were injected subcutaneously into the flanks of the 6-week-old male nude mice. After 3 weeks, all mice showed the development of subcutaneous solid tumors with a volume of approximately 50 mm^3. Each mouse developed two points of solid tumors. All 24 nude mice were randomly divided into 6 groups, with 4 mice in each group, and were subjected to six treatments as follows: Control, PIONs, PIONs@pDNA, NIR, PIONs + NIR, and PIONs@pDNA + NIR. Twenty-five micrograms of PIONs was injected into each solid tumor of the PIONs and PIONs + NIR groups. Twenty-five micrograms of PIONs/pDNA (w/w = 25) was injected into each solid tumor of the PIONs@pDNA and PIONs@pDNA + NIR groups. Tumors in the NIR, PIONs + NIR, and PIONs@pDNA + NIR groups were treated with an NIR laser (808 nm, 1 W/cm^2) for 5 min every two days after the injection. Subsequently, the tumor volumes of all mice were measured every two days by using a caliper for 23 days. Tumor volume was calculated using the formula (3):

$$\text{Volume} = a \times b^2 \times \pi/6 \quad (3)$$

Where a is the length and b is the width of the solid tumor. All the tumor volume data were normalized with that of the control group. After 23 days, all mice were sacrificed, and the tumors were stored in formalin after weighing. The tumor tissues were embedded into paraffin sections, and immunohistochemical analysis, hematoxylin and eosin (H&E) staining, and immunofluorescence staining were performed. TUNEL dye was purchased from Beyotime Biotechnology Corporation (Shanghai, China) and used for apoptotic cells immunofluorescence staining in tumor tissues.

2.13. Statistical analysis

The data were obtained from triplicate experiments and presented as mean ± standard deviation (SD). All the data were analyzed by Student's *t*-test, and the differences between the test and control groups were considered to be significant at $^*p < 0.05$ and very significant at $^{**}p < 0.01$ and $^{***}p < 0.001$.

3. Results and discussion

3.1. Synthesis and characterization of PIONs

To investigate the chemical and physical properties of the nanoagents used in our study, the multifunctional PIONs were prepared according to a modified procedure [43–46], and their properties were determined by several experiments. High-resolution scanning electron microscopy (SEM) micrographs showed that the diameter of PIONs particles was approximately 190 nm (Fig. 1A). In addition, the dynamic light scattering (DLS) technology was used to measure the hydrodynamic diameter distribution of PIONs, and the results show that the PIONs have a stable diameter distribution. (Fig. S1). Besides, the absorption peak of this nanoagent was below approximately 420 nm UV irradiation (Fig. 1C). As shown in Fig. 1B, the magnetic experiment confirmed that this nanomaterial has superparamagnetic property and can be attracted by a magnetic field. As shown in Fig. S2, The photothermal property of PIONs was also tested, and the results indicated that PIONs have high photothermal conversion efficiency (η = 33.8 %). It could increase the medium temperature from 25 °C to 42 °C in 10 min at the concentration of 200 μg/mL (Fig. 1D and E). The photothermal conversion ability increased with the concentration of PIONs, and they showed stability following repeated laser stimulations (Fig. 1F). All these data indicate that PIONs have both excellent photothermal properties and magnetic properties and can be potentially used in clinical diagnosis and treatment.

3.2. Biocompatibility and PTT efficacy of PIONs in vitro and in vivo

The biocompatibility of PIONs, which should be evaluated before the experiments, was determined by the CCK-8 assay. Therefore, we firstly investigated the cytotoxicity of PIONs toward A549 cells. A549 cells were incubated with PIONs for 24 h. The cell viability of A549 cells was still >80 % even at a high concentration (250 μg/mL) of PIONs; this indicated that PIONs showed no significant cytotoxicity toward A549 cells at the tested concentrations (Fig. 2A). However, in the NIR-treated group, the cell viability decreased significantly with the increase in PIONs concentration (Fig. 2A). These results showed that PIONs have less cytotoxic effect on A549 cells and can be used in PTT. We also tested the biocompatibility of PIONs for BEAS-2B cells (Fig. S3), and the results were similar to those obtained for A549 cells.

To combine PTT with GT, plasmid pcDNA3.1-LNC CRYBG3 was constructed and loaded into PIONs. As shown in Fig. 2D, the release rate of the pDNA was measured in PBS with different pH values at room temperature, and the results indicate that the pDNA release rate in acid solvent was a little higher than that in the neutral solvent, which is beneficial to the release of pDNA in the acid tumor environment. As shown in Fig. 2C, the pDNA release from PIONs@pDNA NCs increased when they were exposed to the NIR laser, the release rate of the pDNA was measured using a UV spectrophotometer. The results indicated that the NIR laser can promote pDNA release as compared to natural release.

As NIR laser irradiation was found to promote the separation of pDNA3.1-LNC CRYBG3 from PIONs, we tested the inhibitory effect of PTT combined with GT on the viability of tumor cells. As shown in Fig. 2B, PTT or GT alone could not decrease the viability of cancer cells significantly when the concentration of PIONs was 150 μg/mL. The overexpression of LNC CRYBG3 in A549 cells was verified by qRT-PCR (Figs. S4 and S5). For the PIONs@pDNA group, less than 20 % of

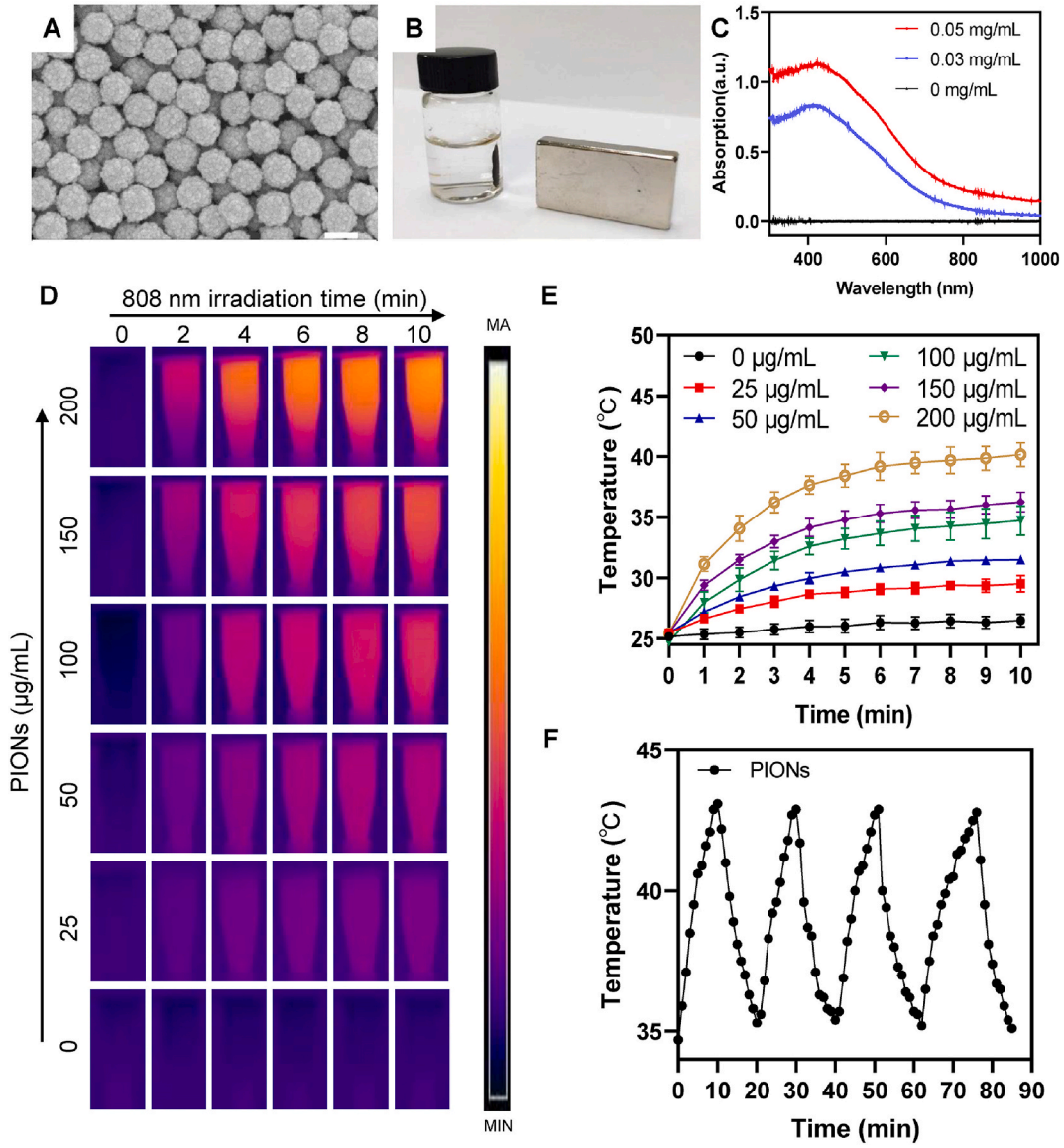

Fig. 1. Characterization of PIONs. (A) High-resolution SEM micrographs show that the PIONs particles adopt a mesoporous morphology with a diameter of 190 nm. Scale bar = 200 nm. (B) Magnetic properties of PIONs. (C) UV absorbance curve of PIONs from 300 nm to 1000 nm. (D) Thermal imaging pictures of PIONs at different concentrations in water under 808 nm laser (1 W/cm^2) irradiation for 10 min. (E) Photothermal heating curves of (D). (F) Heating of a suspension of PIONs in PBS for four laser on/off cycles with an 808 nm NIR laser (1 W/cm^2). The data are shown as mean ± SD. The error bar is derived from triplicate measurements. ***$p < 0.001$, **$p < 0.01$, *$p < 0.05$.

A549 cells were killed without NIR laser irradiation when the PIONs concentration was 150 μg/mL. Approximately 80 % of cells were still alive when they were irradiated with NIR laser alone at the same PIONs concentration. As shown in Fig. S4, the expression of LNC CRYBG3 in the PIONs@pDNA group was approximately 7 times than that of the control group, but the cell viability of the PIONs@pDNA group did not decrease significantly; this implied that LNC CRYBG3 overexpression at such level did not dramatically suppress cell viability. The suppressive effect became significant only when the overexpression level reached over 100 times, as observed in the pDNA (Lipo3000) group. However, the cell viability of PIONs@pDNA + NIR group decreased to 30 %. This indicates that the combination therapy of PTT and GT can significantly decrease cell viability.

The combination curative effect index (CCEI) between the pDNA-mediated GT and PIONs-mediated PTT was calculated according to the following formula (4); the results indicate synergism (CI < 1), additivity (CI = 1), or antagonism (CI > 1) between the two individual therapies:

$$CI = D\alpha/ICX\text{-}\alpha + D\beta/ICX\text{-}\beta \quad (4)$$

α represent PIONs and β represent pDNA; ICX-α and ICX-β are concentrations at which the cell growth inhibition rate reaches X when the two complexes are used alone, and Dα and Dβ are the concentrations of the two complexes when the cell growth rate reaches X if they work together.

The cell viability assay based on the CCK-8 reagent was evaluated as follows:

PTT: the 50 % inhibition rate of cell viability was reached when PIONs were used at the concentration of 450 μg per 1 × 10^6 A549 cells. In the combination therapy, the concentration of PIONs was 300 μg per 1 × 10^6 A549 cells.

GT: the 50 % inhibition rate of cell viability was reached when pDNA was used at the concentration of 1 μg per 1 × 10^6 A549 cells. In the combination therapy, the concentration of pDNA was 0.8 μg per 1 × 10^6 A549 cells.

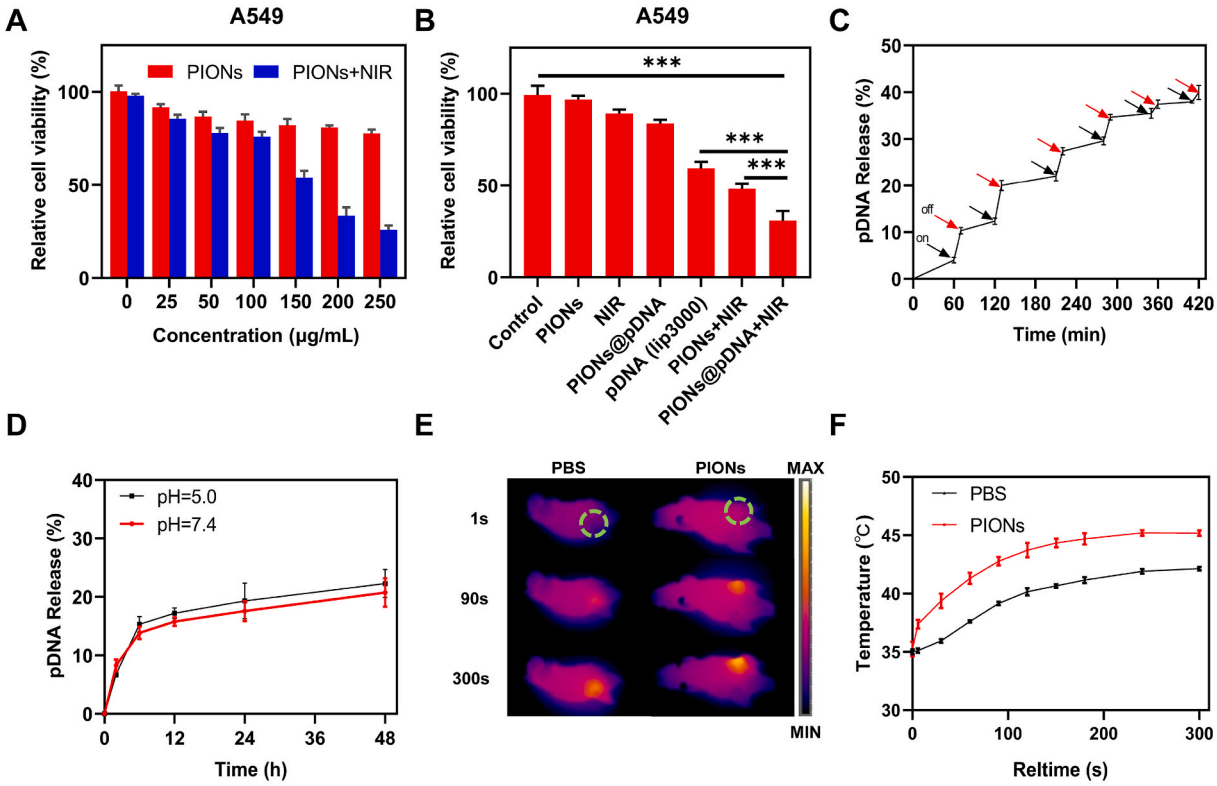

Fig. 2. Biocompatibility and PTT efficacy of PIONs *in vitro* and *in vivo*. (A) Cell viability of A549 cells treated with different concentrations of PIONs with or without 808 nm laser irradiation (1 W/cm^2) for 10 min. (B) Cell viability of A549 cells treated with PIONs or PIONs@pDNA with or without 808 nm laser irradiation (1 W/cm^2, 10 min). (C) pDNA release profile in PBS (pH = 5.0) with intermittent NIR laser irradiation (808 nm, 1 W/cm^2). (D) Cumulative plasmid release profile for PIONs@pDNA measured in PBS (pH = 7.4 or 5.0) at room temperature. (E) Photothermal imaging after injecting PIONs (1 mg/kg) into subcutaneous tumors. (F) is the temperature curve of (E). The tumor was exposed to NIR laser irradiation (808 nm, 1 W/cm^2) for 5 min. The data are expressed as mean ± standard deviation (SD). The error bar is derived from triplicate measurements. ***$p < 0.001$, **$p < 0.01$, *$p < 0.05$.

According to formula (4):

$$CI = 450/300 + 1/0.8 = 2.75 > 1$$

This implies that the combination therapy exhibits better inhibitory effect for A549 cells.

Although we tested the photothermal ability of PIONs *in vitro*, the photothermal effect in live animals may be different. To evaluate this aspect, subcutaneous tumors in nude mice were exposed to NIR laser (1 W/cm^2, 808 nm) for 5 min after PIONs or PBS injection, and the thermal imaging camera was used to record the temperature change of the tumor tissues. We then injected PIONs (25 μL, 1 mg/mL) or PBS (25 μL) into the subcutaneous tumors. Five minutes later, the photothermal images were captured in the same way as mentioned above. The photothermal imaging results indicated that PIONs show photothermal conversion function when exposed to NIR light (Fig. 2E). The local temperature of the tumor increased from 35 °C to 45 °C in 5 min (Fig. 2F).

3.3. Gene therapy basing on LNC CRYBG3 combined with PTT induced apoptosis of A549 cells in vitro

LNC CRYBG3 has been shown to directly bind to G-actin to inhibit its polymerization and formation of contractile rings, resulting in M-phase cell cycle arrest [47], failure of cytokinesis, and cell death. In the present study, we overexpressed LNC CRYBG3 in A549 cells by using the pcDNA3.1-LNC CRYBG3 plasmid. We then used flow cytometry to measure cell apoptosis and found that the apoptosis rate in the combination treatment group increased significantly as compared to that in the single treatment groups (Fig. 3A and B). The western blotting experiment also showed that the expression of apoptotic protein Bax and cleaved-caspased3 was increased, while caspase3 and anti-apoptosis protein Bcl-2 was decreased after combination treatment (Fig. S6). The results showed that LNC CRYBG3-induced cell apoptosis was significantly aggravated by PIONs and NIR.

F-actin is the main component of the cytoskeleton and its polymerization from G-actin is a dynamic process. In Fig. 3C, Western blot analysis shows the F-actin to G-actin ratio decreased when LNC CRYBG3 was delivered into A549 cells, which means the polymerization of F-actin by G-actin was suppressed by LNC CRYBG3. Jasplakinolide was used to promote the F-actin assembly to be a positive control. As shown in Fig. 3D, A549 cells in the PIONs and PIONs + NIR groups exhibited normal cell cytoskeleton structure as demonstrated by phalloidin staining; this suggested that PIONs do not affect the morphology of cell cytoskeleton. We then measured the percentage of binucleated cells and found that the percentage of these cells increased more significantly in the combination treatment groups as compared to that in the single treatment groups (Fig. 3G). We also noted that the delivery of pDNA into cells through PIONs caused high degradation of cell cytoskeleton. Moreover, NIR treatment aggravated the degradation of cell cytoskeleton induced by LNC CRYBG3.

As shown in Fig. 3E, F, H and I, the lysosomal escape capability of PIONs facilitated by NIR laser was observed under laser scanning confocal microscope. The lysosome of A549 cells was stained with LysoTracker Red and the nucleus was stained with DAPI. The overlay of red and green fluorescence indicated that the PIONs-Cy5.5 were located in lysosomes and the separation of green and red fluorescence indicated that the PIONs-Cy5.5 escaped from lysosomes to cytoplasm. In the control group, the PIONs-Cy5.5 was captured by lysosomes after 2 h incubation with little releasement. Relatively, when treated with NIR (808 nm, 1 W/cm^2) for 10 min, the releasement of PIONs from lysosomes increased obviously post irradiation. These data illustrate that the

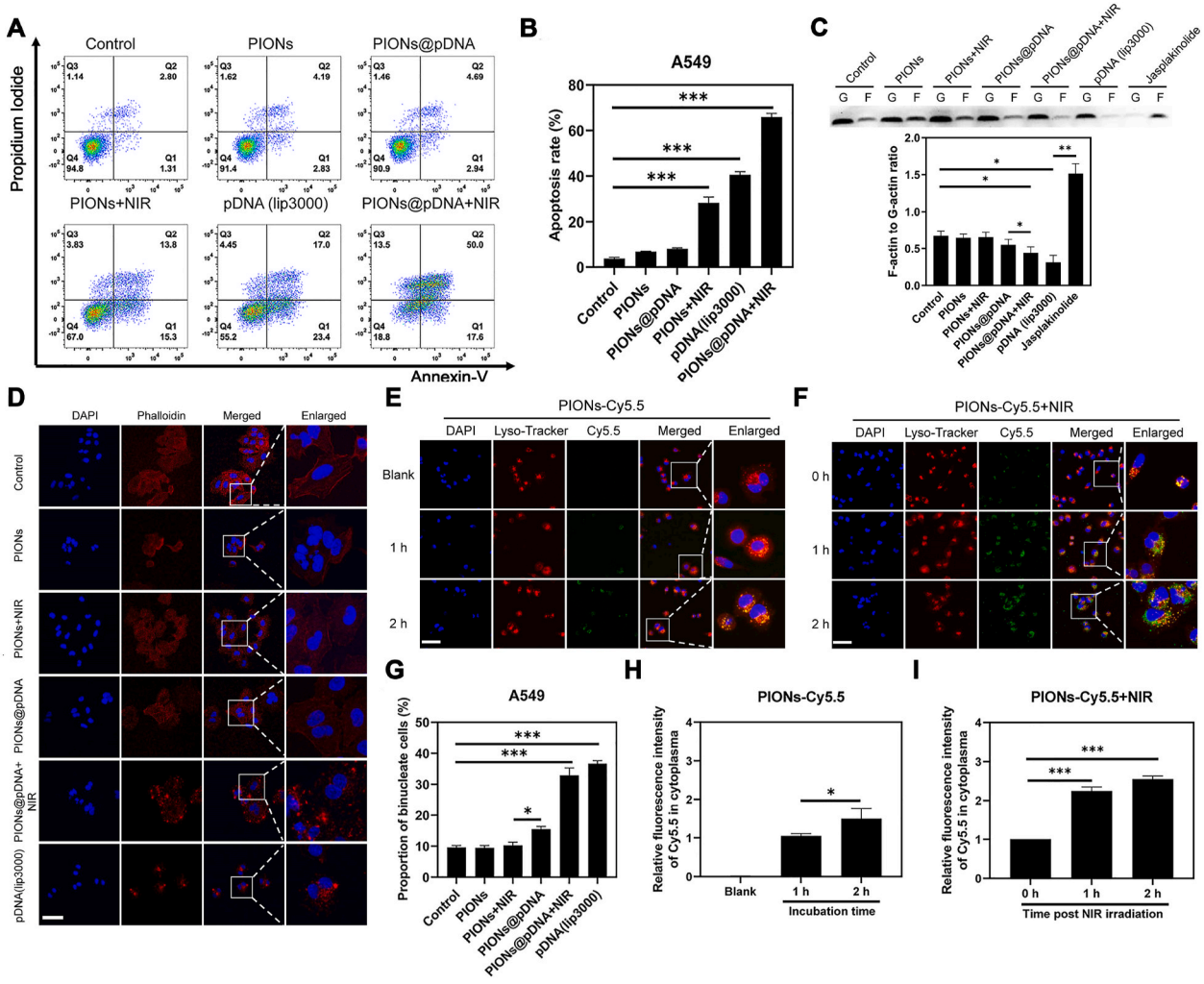

Fig. 3. PIONs mediated cell apoptosis, cytoskeleton depolymerization and lysosomal escape under NIR irradiation. (A) Apoptotic cells caused by LNC CRYBG3 and PTT. (B) The apoptosis rate in (A) increased significantly in the combination treatment. (C) F-actin and G-actin protein levels in the A549 cells in different groups. (D) LNC CRYBG3 overexpression influenced the normal structure of the cytoskeleton of A549 cells as demonstrated by phalloidin staining. Scale bar = 50 μm. (E) Laser scanning confocal microscope images of A549 cells incubated with PIONs-Cy5.5 (200 μg/mL) for 2 h. Scale bar = 50 μm. (F) Laser scanning confocal microscope images of A549 cells incubated with PIONs-Cy5.5 (200 μg/mL) for 2 h after 10 min NIR (808 nm, 1 W/cm^2) irradiation. A549 cells were incubated with PIONs-Cy5.5 (200 μg/mL) for 2 h and then exposed to the NIR irradiation (1 W/cm^2) for 5 min and the laser scanning confocal microscope images were taken at different time points post irradiation. Scale bar = 50 μm. (G) The percentage of binucleated cells was also increased following the combination treatment. (H) The quantitive data of (E). (I) Quantitive data of (F). Nuclei of cells were stained by 4′,6-diamidino-2-phenylindole (DAPI) and lysosomes were stained with LysoTracker Red. PIONs were labeled with Cy5.5. The data are expressed as mean ± standard deviation (SD). The error bar is derived from triplicate measurements. ***$p < 0.001$, **$p < 0.01$, *$p < 0.05$. (For interpretation of the references to colour in this figure legend, the reader is referred to the Web version of this article.)

NIR laser can promote lysosomal escape of PIONs in A549 cells, thus enhance the expression of LNC CRYBG3.

3.4. Imaging property of PIONs in vitro and in vivo

The distribution of most nanomaterials with photothermal properties can be detected by PA imaging [48,49], which can serve as a complementary tool for MRI with insufficient resolution [50–53]. To further test the diagnosis and treatment potential of PIONs in clinical application, we used three different approaches to measure the imaging property of PIONs both *in vivo* and *in vitro*. First, we used a PA imaging machine to obtain the PA signal of PIONs *in vitro*. As shown in Fig. 4A and C and S7, the PA signal increased linearly with the increase of PIONs concentration under different wavelengths. The results indicated that PIONs have an excellent and stable PA imaging ability. For application in clinical diagnosis, we also tested the magnetic resonance imaging property of PIONs *in vivo*, and the results were similar to those obtained for PA imaging. In the *in vitro* tests, the MRI signal showed a linear relationship with the concentration of PIONs (Fig. 4B and D). The relaxation rate (r_2) of PIONs was approximately 257.1 mM^{-1} s^{-1} according to our calculations. This implied that PIONs have a good ability to be imaged by MRI and can be used in clinical diagnosis. Thus, the combination of PA imaging technology and MRI can overcome the problem of insufficient resolution to a certain extent, which is a current research hotspot [50,54].

We then tested the imaging ability of PIONs *in vivo* to investigate whether this nanoagent can be used in clinical diagnosis. The PA machine was also used to acquire the PA signal *in vivo*. PIONs (25 μL, 1 mg/mL) were injected into the tumor tissues of mice before PA scanning. Before and after the injection, the mice were anesthetized with gaseous ether and scanned in the PA machine. The PA image shows that the PIONs could be detected *in vivo* even at a low concentration (Fig. 4E and S8). The same approach was used to test the MR imaging ability of PIONs *in vitro*. The MR image also showed that PIONs could be detected,

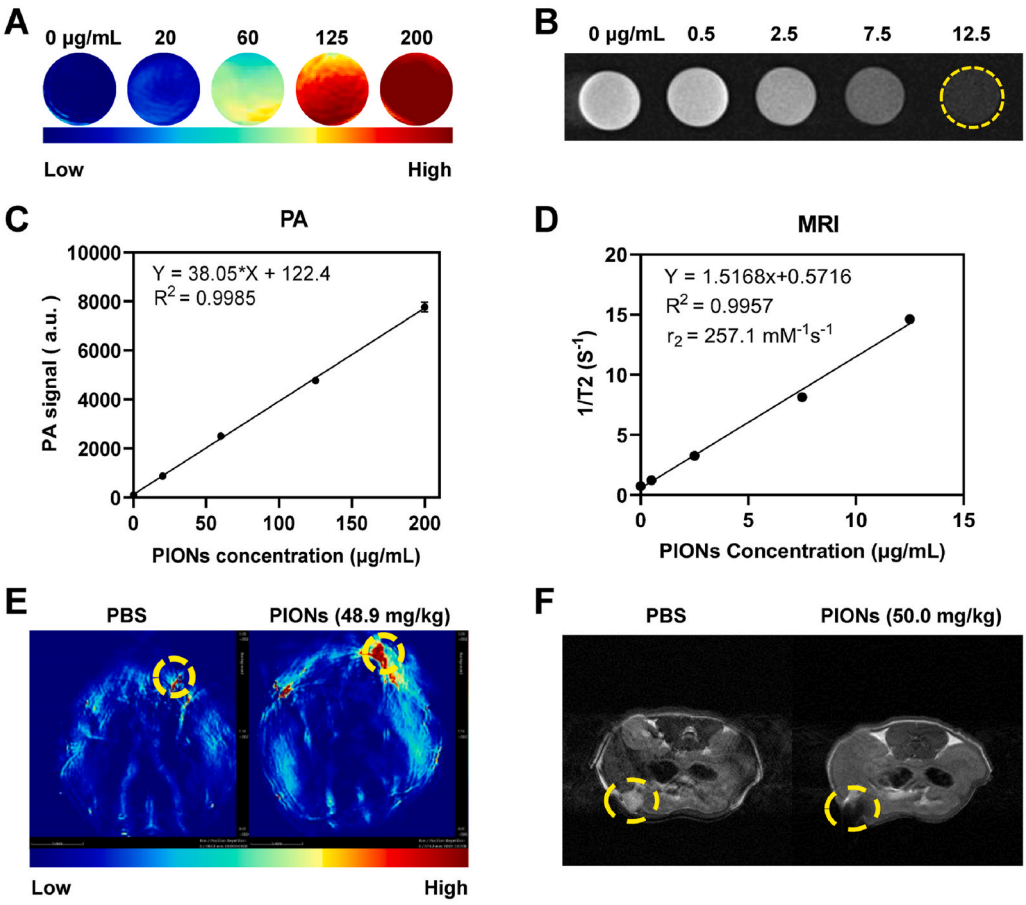

Fig. 4. Imaging Property of PIONs *in vitro* and *in vivo*. (A) PA imaging and (B) MR imaging of PIONs at different concentrations. (C) The PA signal curve of PIONs at different concentrations in (A) shows a linear relation. (D) The 1/T2 of PIONs at different concentrations in (B) shows a linear relation, and the relaxation rate r_2 = 257.1 mM^{-1} s^{-1} means an excellent MRI imaging ability. (E) PA imaging and (F) MR imaging of PIONs *in vivo*. The data are expressed as mean ± standard deviation (SD). The error bar is derived from triplicate measurements. ***$p < 0.001$, **$p < 0.01$, *$p < 0.05$.

and the signal was quite higher than that before injection (Fig. 4F and S9). All these data indicated that PIONs have an excellent imaging ability in both *in vivo* and *in vitro* conditions; this implied that they have the potential to be used as a clinical contrast agent in the future.

3.5. Combination of PTT and GT inhibits tumor growth significantly in vivo

To further investigate the *in vivo* efficacy of the combination therapy, nude mice with transplanted tumors of approximately 50 mm^3 derived from A549 cells were randomly divided into six groups and subcutaneously injected with PBS, PIONs, or PIONs@pDNA at the dose of 1 mg/kg PIONs or 1 mg/kg PIONs@pDNA (pDNA/PIONs = 1/5), followed with or without 5 min NIR laser irradiation (808 nm, 1 W/cm^2) post-injection (Fig. 5A). The tumor growth was almost completely suppressed in the group treated with PIONs@pDNA + NIR irradiation (Fig. 5B and C). In contrast, the PIONs, PIONs@pDNA, and NIR groups did not show a significant antitumor effect. The bodyweight of mice in the different groups did not show a dramatic change in the experimental duration of 23 days (Fig. 5D). The blood routine test and H&E stain of main organs of combination therapy treated mice also showed no obvious change compared to the control group. (Figs. S10 and S11). These results suggested that combination therapy has few side effects on the whole body. The volume and weight of the dissected tumors were most significantly reduced in the combination therapy group (Fig. 5B and E). We used phalloidin staining to determine cytoskeletal changes in cells (Fig. 5F) and the TUNEL immunofluorescence staining to determine the apoptosis rate of tumor cells (Fig. 5G). The results indicated that the combination treatment caused more cell apoptosis than that observed in the other groups; moreover, the cytoskeleton morphology was also most apparently changed in the combination treatment group. Compared to the control group, the PIONs@pDNA + NIR group showed more apparent damage and inflammation as observed in H&E staining images of tumors (Fig. 5G). Ki-67 staining suggested downregulation of the cell proliferation level in the combination treatment group as compared to that in the control group (Fig. 5G). All these data indicated that the combination therapy had higher tumor inhibition efficiency through induction of cell apoptosis.

4. Conclusion

Heavy ion irradiation is receiving increasing attention in the field of radiotherapy, and it is considered as the most ideal radiation therapy in the 21st century. However, the high cost of this therapy limits its widespread clinical application. Moreover, the possible side effects due to the high linear energy transfer (LET) radiation deposited in normal tissues raise concerns about the safety of this therapy [55–57]. In our previous study, we found that LNC CRYBG3 was upregulated in lung cancer cells when exposed to both X-rays and carbon ion radiation, but the upregulation following X-ray exposure was not as markedly as that following carbon ion radiation. Further investigations showed that the upregulation of LNC CRYBG3 can alter the cytoskeleton by interacting with G-actin, thereby causing failure of cell mitosis through inhibition of contractile ring formation. Finally, the double-nucleated cells were committed to apoptosis because of genomic instability [35,36]. Thus, LNC CRYBG3 shows clinical potential as a tumor inhibitory molecule to simulate the effect of heavy ion irradiation therapy. LNC CRYBG3, however, cannot target tumor tissues specifically. PIONs have been used as a delivery platform for chemotherapeutic drugs in some research studies. In the present study, we investigated for the first time the potential of PIONs to deliver tumor-suppressive lncRNA for gene therapy. The use of PIONs can make good use of its PTT property because of the

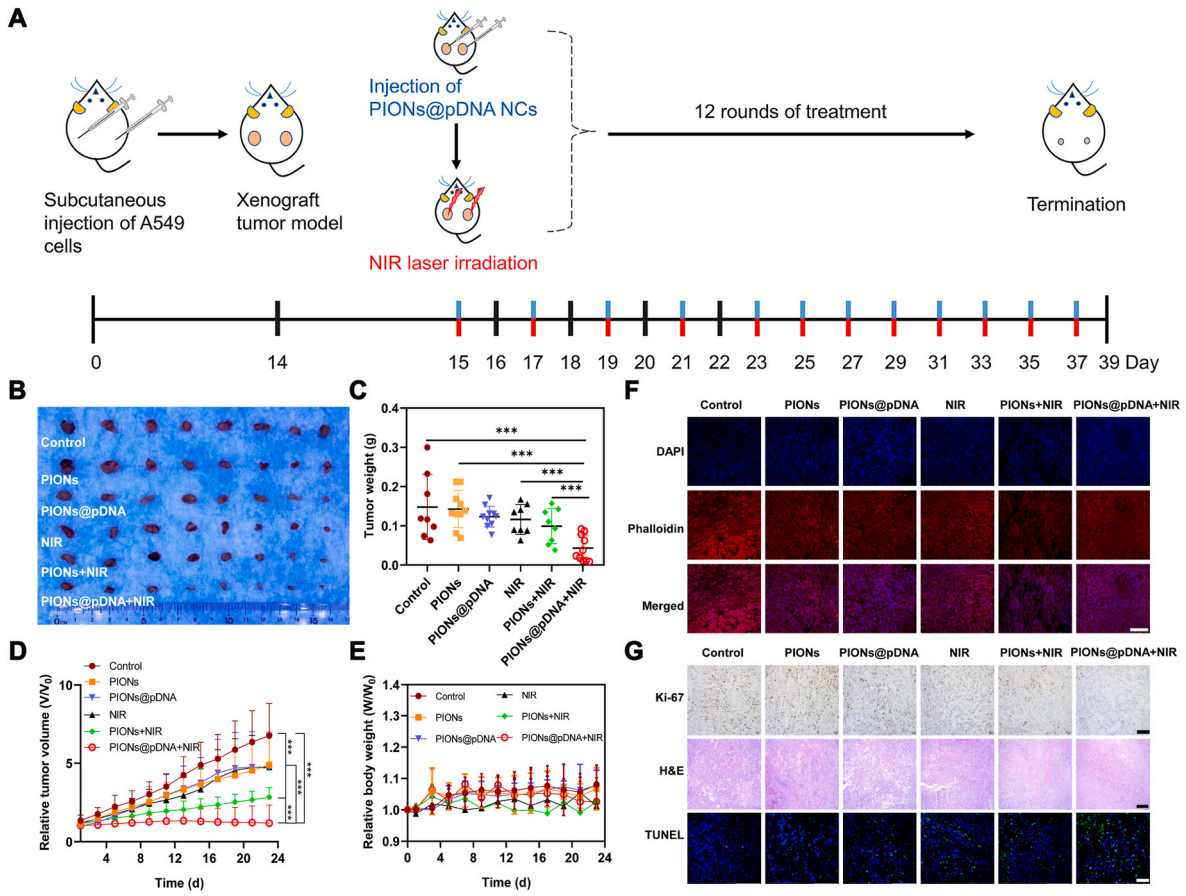

Fig. 5. Combination treatment of PTT and GT *in vivo*. (A) Schematic illustration of combination therapy of nude mice. (B) Tumors dissected from mice after 23 days post-treatment and (C) Tumor weight in different treatment groups. (D) Relative tumor volume change during 23 days. (E) Relative body weight change of mice in 23 days. (F) Phalloidin staining of tumor slices collected from mice post various treatments (day 23). The cytoskeleton protein was stained with phalloidin (red) and the nucleus was stained with DAPI (blue). Scale bar = 50 μm. (G) Microscopy images of Ki-67-stained (scale bar = 100 μm), H&E-stained (scale bar = 200 μm), and TUNEL-stained (scale bar = 50 μm) tumor slices collected from different groups of mice. In Ki-67 image, the brown point presents the Ki-67 positive cells. In the TUNEL image, the nucleus was stained with DAPI (blue) and apoptosis cells were stained with TUNEL (green). The data are expressed as mean ± standard deviation (SD). The error bar is based on 4 replicates. $^{***}p < 0.001$, $^{**}p < 0.01$, $^{*}p < 0.05$. (For interpretation of the references to colour in this figure legend, the reader is referred to the Web version of this article.)

magnetic and photothermal properties of PIONs, which can help to efficiently deliver and release LNC CRYBG3 to tumor tissues.

By using PIONs, we successfully delivered the pcDNA3.1-LNC CRYBG3 plasmid into A549 lung cancer cells and overexpressed the tumor-killing LNC CRYBG3. Although the efficiency of this approach was lower than that of the traditional transfection reagent such as Lipo3000 and adenovirus, it was adequate to kill cancer cells. PIONs could be detected in tumor tissues under MRI because of their magnetic property; this indicates that we could guide PIONs into tumor tissues more accurately than the traditional GT. Moreover, if we expose the PIONs to NIR laser, the heating effect created by PIONs can also help to kill cancer cells. The PIONs@pDNA was endocytosed by cells and captured by lysosomes. When cells were exposed to the 808 nm NIR laser, the photothermal effect promoted the escape of PIONs@pDNA from lysosomes. Meanwhile, the increased temperature promoted the release of pDNA from PIONs. Finally, the pDNA could be highly released to cytoplasm and entered into the nucleus to express the LNC CRYBG3, which induced the cytoskeleton depolymerization.

In summary, the GT based on LNC CRYBG3 and PTT based on PIONs can act synergistically and increase tumor control rate significantly. This new adjuvant therapy has the potential to be a good choice in the future clinical treatment of tumors.

CRediT authorship contribution statement

Hao Huang: Investigation, Methodology, Data curation, Formal analysis, Writing – original draft. **Guotao Yuan:** Investigation, Formal analysis, Writing – original draft. **Ying Xu:** Investigation, Visualization, Writing – review & editing. **Yuan Gao:** Investigation. **Qiulian Mao:** Investigation, Methodology, Data curation. **Yin Zhang:** Writing – review & editing. **Lu Bai:** Investigation. **Weijie Li:** Methodology, Formal analysis, Data curation. **Anqing Wu:** Methodology. **Wentao Hu:** Conceptualization, Supervision, Writing – review & editing. **Yue Pan:** Funding acquisition, Supervision, Conceptualization, Writing – review & editing. **Guangming Zhou:** Conceptualization, Writing – review & editing, Supervision, Funding acquisition, Project administration.

Declaration of competing interest

The authors declare that they have no known competing financial interests or personal relationships that could have appeared to influence the work reported in this paper.

Acknowledgements

This work was supported by the National Key R&D program of China (2018YFC0115704, 2018YFB1105700); the Guangdong Science and

Technology Department (2020B1212060018, 2020B1212030004); the Guangdong Basic and Applied Basic Research Foundation for Distinguished Young Scholars(2020B1515020027); the grant from Guangzhou Science and Technology Bureau (202002020070, 202102010181, 202102010007).

Appendix A. Supplementary data

Supplementary data to this article can be found online at https://doi.org/10.1016/j.bioactmat.2021.07.025.

References

[1] F. Li, W. Yu, J. Zhang, Y. Dong, X. Ding, X. Ruan, Z. Gu, D. Yang, Spatiotemporally programmable cascade hybridization of hairpin DNA in polymeric nanoframework for precise siRNA delivery, Nat. Commun. 12 (1) (2021) 1138, https://doi.org/10.1038/s41467-021-21442-7.

[2] P. Zheng, B. Ding, R. Shi, Z. Jiang, W. Xu, G. Li, J. Ding, X. Chen, A multichannel Ca nanomodulator for multilevel mitochondrial destruction-mediated cancer therapy, Adv Mater 33 (15) (2021), e2007426, https://doi.org/10.1002/adma.202007426.

[3] P. Zheng, Y. Liu, J. Chen, W. Xu, G. Li, J. Ding, Targeted pH-responsive polyion complex micelle for controlled intracellular drug delivery, Chin. Chem. Lett. 31 (5) (2020) 1178–1182, https://doi.org/10.1016/j.cclet.2019.12.001.

[4] X. Feng, W. Xu, X. Xu, G. Li, J. Ding, X. Chen, Cystine proportion regulates fate of polypeptide nanogel as nanocarrier for chemotherapeutics, Sci. China Chem. 64 (2) (2021) 293–301, https://doi.org/10.1007/s11426-020-9884-6.

[5] S. Huo, N. Gong, Y. Jiang, F. Chen, H. Guo, Y. Gan, Z. Wang, A. Herrmann, X. J. Liang, Gold-DNA nanosunflowers for efficient gene silencing with controllable transformation, Science advances 5 (10) (2019) eaaw6264, https://doi.org/10.1126/sciadv.aaw6264.

[6] Y. Pan, X. Du, F. Zhao, B. Xu, Magnetic nanoparticles for the manipulation of proteins and cells, Chem. Soc. Rev. 41 (7) (2012) 2912–2942, https://doi.org/10.1039/c2cs15315g.

[7] X. Tian, L. Zhang, M. Yang, L. Bai, Y. Dai, Z. Yu, Y. Pan, Functional magnetic hybrid nanomaterials for biomedical diagnosis and treatment, Wiley Interdiscip Rev Nanomed Nanobiotechnol 10 (1) (2018), https://doi.org/10.1002/wnan.1476.

[8] D.P. Madio, P. van Gelderen, D. DesPres, A.W. Olson, J.A. de Zwart, T.W. Fawcett, N.J. Holbrook, M. Mandel, C.T. Moonen, On the feasibility of MRI-guided focused ultrasound for local induction of gene expression, J. Magn. Reson. Imag. 8 (1) (1998) 101–104, https://doi.org/10.1002/jmri.1880080120.

[9] J. Estelrich, M.A. Busquets, Iron oxide nanoparticles in photothermal therapy, Molecules 23 (7) (2018), https://doi.org/10.3390/molecules23071567.

[10] R.S. Riley, E.S. Day, Gold nanoparticle-mediated photothermal therapy: applications and opportunities for multimodal cancer treatment, Wiley Interdiscip Rev Nanomed Nanobiotechnol 9 (4) (2017), https://doi.org/10.1002/wnan.1449.

[11] Y. Hu, H. Hu, J. Yan, C. Zhang, Y. Li, M. Wang, W. Tan, J. Liu, Y. Pan, Multifunctional porous iron oxide nanoagents for MRI and photothermal/chemo synergistic therapy, Bioconjugate Chem. 29 (4) (2018) 1283–1290, https://doi.org/10.1021/acs.bioconjchem.8b00052.

[12] M. Chang, Z. Hou, M. Wang, C. Li, J. Lin, Recent advances in hyperthermia therapy-based synergistic immunotherapy, Adv Mater 33 (4) (2021), e2004788, https://doi.org/10.1002/adma.202004788.

[13] M. Chang, Z. Hou, M. Wang, M. Wang, P. Dang, J. Liu, M. Shu, B. Ding, A.A. Al Kheraif, C. Li, J. Lin, Cu2 MoS4/Au heterostructures with enhanced catalase-like activity and photoconversion efficiency for primary/metastatic tumors eradication by phototherapy-induced immunotherapy, Small 16 (14) (2020), e1907146, https://doi.org/10.1002/smll.201907146.

[14] O. Kepp, A. Marabelle, L. Zitvogel, G. Kroemer, Oncolysis without viruses - inducing systemic anticancer immune responses with local therapies, Nat. Rev. Clin. Oncol. 17 (1) (2020) 49–64, https://doi.org/10.1038/s41571-019-0272-7.

[15] L. Rong, Y. Zhang, W.-S. Li, Z. Su, J.I. Fadhil, C. Zhang, Iron chelated melanin-like nanoparticles for tumor-associated macrophage repolarization and cancer therapy, Biomaterials 225 (2019) 119515, https://doi.org/10.1016/j.biomaterials.2019.119515.

[16] S. Jiang, A.A. Eltoukhy, K.T. Love, R. Langer, D.G. Anderson, Lipidoid-Coated iron oxide nanoparticles for efficient DNA and siRNA delivery, Nano Lett. 13 (3) (2013) 1059–1064, https://doi.org/10.1021/nl304287a.

[17] R.Y. Huang, Y.H. Lin, S.Y. Lin, Y.N. Li, C.S. Chiang, C.W. Chang, Magnetic ternary nanohybrids for nonviral gene delivery of stem cells and applications on cancer therapy, Theranostics 9 (8) (2019) 2411–2423, https://doi.org/10.7150/thno.29326.

[18] J. Shi, P.W. Kantoff, R. Wooster, O.C. Farokhzad, Cancer nanomedicine: progress, challenges and opportunities, Nat. Rev. Canc. 17 (1) (2016) 20–37, https://doi.org/10.1038/nrc.2016.108.

[19] M.A. Islam, Y. Xu, W. Tao, J.M. Ubellacker, M. Lim, D. Aum, G.Y. Lee, K. Zhou, H. Zope, M. Yu, W. Cao, J.T. Oswald, M. Dinarvand, M. Mahmoudi, R. Langer, P. W. Kantoff, O.C. Farokhzad, B.R. Zetter, J. Shi, Restoration of tumour-growth suppression in vivo via systemic nanoparticle-mediated delivery of PTEN mRNA, Nat Biomed Eng 2 (11) (2018) 850–864, https://doi.org/10.1038/s41551-018-0284-0.

[20] N. Kong, W. Tao, X. Ling, J. Wang, Y. Xiao, S. Shi, X. Ji, A. Shajii, S.T. Gan, N. Y. Kim, D.G. Duda, T. Xie, O.C. Farokhzad, J. Shi, Synthetic mRNA nanoparticle-mediated restoration of p53 tumor suppressor sensitizes -deficient cancers to mTOR inhibition, Sci. Transl. Med. 11 (523) (2019), https://doi.org/10.1126/scitranslmed.aaw1565.

[21] X. Mu, J. Li, S. Yan, H. Zhang, W. Zhang, F. Zhang, J. Jiang, siRNA delivery with stem cell membrane-coated magnetic nanoparticles for imaging-guided photothermal therapy and gene therapy, ACS Biomater. Sci. Eng. 4 (11) (2018) 3895–3905, https://doi.org/10.1021/acsbiomaterials.8b00858.

[22] C. Xu, K. Pu, Second near-infrared photothermal materials for combinational nanotheranostics, Chem. Soc. Rev. 50 (2) (2021) 1111–1137, https://doi.org/10.1039/d0cs00664e.

[23] Y. Zhang, C. Xu, X. Yang, K. Pu, Photoactivatable protherapeutic nanomedicine for cancer, Adv Mater 32 (34) (2020), e2002661, https://doi.org/10.1002/adma.202002661.

[24] X. Liu, M. Xu, Y. Zhao, X. Chen, X. Zhu, C. Wei, S. Zhao, J. Liu, X. Qin, Correction: Flower-like gold nanoparticles for enhanced photothermal anticancer therapy by the delivery of pooled siRNA to inhibit heat shock stress response, J. Mater. Chem. B 7 (9) (2019) 1510, https://doi.org/10.1039/c9tb90022e.

[25] N. Tran, T.J. Webster, Magnetic nanoparticles: biomedical applications and challenges, J. Mater. Chem. 20 (40) (2010), https://doi.org/10.1039/c0jm00994f.

[26] D. Shao, J. Li, X. Zheng, Y. Pan, Z. Wang, M. Zhang, Q.X. Chen, W.F. Dong, L. Chen, Janus "nano-bullets" for magnetic targeting liver cancer chemotherapy, Biomaterials 100 (2016) 118–133, https://doi.org/10.1016/j.biomaterials.2016.05.030.

[27] Y. Zhang, Y. Shen, X. Teng, M. Yan, H. Bi, P.C. Morais, Mitochondria-targeting nanoplatform with fluorescent carbon dots for long time imaging and magnetic field-enhanced cellular uptake, ACS Appl. Mater. Interfaces 7 (19) (2015) 10201–10212, https://doi.org/10.1021/acsami.5b00405.

[28] J. Dang, H. Ye, Y. Li, Q. Liang, X. Li, L. Yin, Multivalency-assisted membrane-penetrating siRNA delivery sensitizes photothermal ablation via inhibition of tumor glycolysis metabolism, Biomaterials 223 (2019), 119463, https://doi.org/10.1016/j.biomaterials.2019.119463.

[29] B.K. Wang, X.F. Yu, J.H. Wang, Z.B. Li, P.H. Li, H. Wang, L. Song, P.K. Chu, C. Li, Gold-nanorods-siRNA nanoplex for improved photothermal therapy by gene silencing, Biomaterials 78 (2016) 27–39, https://doi.org/10.1016/j.biomaterials.2015.11.025.

[30] M. Wu, Q. Meng, Y. Chen, Y. Du, L. Zhang, Y. Li, L. Zhang, J. Shi, Large-pore ultrasmall mesoporous organosilica nanoparticles: micelle/precursor co-templating assembly and nuclear-targeted gene delivery, Adv Mater 27 (2) (2015) 215–222, https://doi.org/10.1002/adma.201404256.

[31] F. Ding, X. Gao, X. Huang, H. Ge, M. Xie, J. Qian, J. Song, Y. Li, X. Zhu, C. Zhang, Polydopamine-coated nucleic acid nanogel for siRNA-mediated low-temperature photothermal therapy, Biomaterials 245 (2020), 119976, https://doi.org/10.1016/j.biomaterials.2020.119976.

[32] Y. Lyu, S. He, J. Li, Y. Jiang, H. Sun, Y. Miao, K. Pu, A photolabile semiconducting polymer nanotransducer for near-infrared regulation of CRISPR/Cas9 gene editing, Angew Chem. Int. Ed. Engl. 58 (50) (2019) 18197–18201, https://doi.org/10.1002/anie.201909264.

[33] T.G. Phan, P.I. Croucher, The dormant cancer cell life cycle, Nat. Rev. Canc. 20 (7) (2020) 398–411, https://doi.org/10.1038/s41568-020-0263-0.

[34] P.L. Bedard, D.M. Hyman, M.S. Davids, L.L. Siu, Small molecules, big impact: 20 years of targeted therapy in oncology, Lancet 395 (10229) (2020) 1078–1088, https://doi.org/10.1016/s0140-6736(20)30164-1.

[35] H. Pei, W. Hu, Z. Guo, H. Chen, J. Ma, W. Mao, B. Li, A. Wang, J. Wan, J. Zhang, J. Nie, G. Zhou, T.K. Hei, Long noncoding RNA CRYBG3 blocks cytokinesis by directly binding G-actin, Canc. Res. 78 (16) (2018) 4563–4572, https://doi.org/10.1158/0008-5472.CAN-18-0988.

[36] W. Mao, Z. Guo, Y. Dai, J. Nie, B. Li, H. Pei, G. Zhou, LNC CRYBG3 inhibits tumor growth by inducing M phase arrest, J. Canc. 10 (12) (2019) 2764–2770, https://doi.org/10.7150/jca.31703.

[37] H.S. Jung, P. Verwilst, A. Sharma, J. Shin, J.L. Sessler, J.S. Kim, Organic molecule-based photothermal agents: an expanding photothermal therapy universe, Chem. Soc. Rev. 47 (7) (2018) 2280–2297, https://doi.org/10.1039/c7cs00522a.

[38] H. Wang, J. Chang, M. Shi, W. Pan, N. Li, B. Tang, A dual-targeted organic photothermal agent for enhanced photothermal therapy, Angew Chem. Int. Ed. Engl. 58 (4) (2019) 1057–1061, https://doi.org/10.1002/anie.201811273.

[39] Z. Liu, L. Cheng, L. Zhang, Z. Yang, Z. Liu, J. Fang, Sub-100 nm hollow Au-Ag alloy urchin-shaped nanostructure with ultrahigh density of nanotips for photothermal cancer therapy, Biomaterials 35 (13) (2014) 4099–4107, https://doi.org/10.1016/j.biomaterials.2014.01.053.

[40] L.F. Fajardo, Pathological effects of hyperthermia in normal tissues, Canc. Res. 44 (10 Suppl) (1984) 4826s–4835s.

[41] D.K. Roper, W. Ahn, M. Hoepfner, Microscale heat transfer transduced by surface plasmon resonant gold nanoparticles, J Phys Chem C Nanomater Interfaces 111 (9) (2007) 3636–3641, https://doi.org/10.1021/jp064341w.

[42] A. Holzinger, Jasplakinolide: an actin-specific reagent that promotes actin polymerization, Methods Mol. Biol. 586 (2009) 71–87, https://doi.org/10.1007/978-1-60761-376-3_4.

[43] R. Dai, Y. Hang, Q. Liu, S. Zhang, L. Wang, Y. Pan, H. Chen, Improved neural differentiation of stem cells mediated by magnetic nanoparticle-based biophysical stimulation, J. Mater. Chem. B 7 (26) (2019) 4161–4168, https://doi.org/10.1039/c9tb00678h.

[44] L. Wang, J. Wu, Y. Hu, C. Hu, Y. Pan, Q. Yu, H. Chen, Using porous magnetic iron oxide nanomaterials as a facile photoporation nanoplatform for macromolecular delivery, J. Mater. Chem. B 6 (27) (2018) 4427–4436, https://doi.org/10.1039/c8tb01026a.

[45] C. Hu, J. Wu, T. Wei, W. Zhan, Y. Qu, Y. Pan, Q. Yu, H. Chen, A supramolecular approach for versatile biofunctionalization of magnetic nanoparticles, J. Mater. Chem. B 6 (15) (2018) 2198–2203, https://doi.org/10.1039/c8tb00490k.
[46] Y. Oh, J.Y. Je, M.S. Moorthy, H. Seo, W.H. Cho, pH and NIR-light-responsive magnetic iron oxide nanoparticles for mitochondria-mediated apoptotic cell death induced by chemo-photothermal therapy, Int. J. Pharm. 531 (1) (2017) 1–13, https://doi.org/10.1016/j.ijpharm.2017.07.014.
[47] W. Pei, W. Hu, Z. Chai, G. Zhou, Current status of space radiobiological studies in China, Life Sci. Space Res. 22 (2019) 1–7, https://doi.org/10.1016/j.lssr.2019.05.001.
[48] S. He, Y. Jiang, J. Li, K. Pu, Semiconducting polycomplex nanoparticles for photothermal ferrotherapy of cancer, Angew Chem. Int. Ed. Engl. 59 (26) (2020) 10633–10638, https://doi.org/10.1002/anie.202003004.
[49] P. Zheng, B. Ding, Z. Jiang, W. Xu, G. Li, J. Ding, X. Chen, Ultrasound-augmented mitochondrial calcium ion overload by calcium nanomodulator to induce immunogenic cell death, Nano Lett. 21 (5) (2021) 2088–2093, https://doi.org/10.1021/acs.nanolett.0c04778.
[50] I. Kosik, M. Brackstone, A. Kornecki, A. Chamson-Reig, P. Wong, J.J.L. Carson, Lipid-weighted intraoperative photoacoustic tomography of breast tumors: volumetric comparison to preoperative MRI, Photoacoustics 18 (2020) 100165, https://doi.org/10.1016/j.pacs.2020.100165.
[51] X. Zhang, J. Tang, C. Li, Y. Lu, L. Cheng, J. Liu, A targeting black phosphorus nanoparticle based immune cells nano-regulator for photodynamic/photothermal and photo-immunotherapy, Bioact Mater 6 (2) (2021) 472–489, https://doi.org/10.1016/j.bioactmat.2020.08.024.
[52] R. Ouyang, P. Cao, P. Jia, H. Wang, T. Zong, C. Dai, J. Yuan, Y. Li, D. Sun, N. Guo, Y. Miao, S. Zhou, Bistratal Au@BiS nanobones for excellent NIR-triggered/multimodal imaging-guided synergistic therapy for liver cancer, Bioact Mater 6 (2) (2021) 386–403, https://doi.org/10.1016/j.bioactmat.2020.08.023.
[53] Z. Fan, H. Liu, Y. Xue, J. Lin, Y. Fu, Z. Xia, D. Pan, J. Zhang, K. Qiao, Z. Zhang, Y. Liao, Reversing cold tumors to hot: an immunoadjuvant-functionalized metal-organic framework for multimodal imaging-guided synergistic photo-immunotherapy, Bioact Mater 6 (2) (2021) 312–325, https://doi.org/10.1016/j.bioactmat.2020.08.005.
[54] D. Zheng, C. Wan, H. Yang, L. Xu, Q. Dong, C. Du, J. Du, F. Li, Her2-Targeted multifunctional nano-theranostic platform mediates tumor microenvironment remodeling and immune activation for breast cancer treatment, Int. J. Nanomed. 15 (2020) 10007–10028, https://doi.org/10.2147/IJN.S271213.
[55] P. Blanchard, G.B. Gunn, A. Lin, R.L. Foote, N.Y. Lee, S.J. Frank, Proton therapy for head and neck cancers, Semin. Radiat. Oncol. 28 (1) (2018) 53–63, https://doi.org/10.1016/j.semradonc.2017.08.004.
[56] W. Tinganelli, M. Durante, Carbon ion radiobiology, Cancers 12 (10) (2020), https://doi.org/10.3390/cancers12103022.
[57] T.D. Malouff, A. Mahajan, R.W. Mutter, S. Krishnan, B.S. Hoppe, C. Beltran, D. M. Trifiletti, L.A. Vallow, Carbon ion radiation therapy in breast cancer: a new frontier, Breast Canc. Res. Treat. 181 (2) (2020) 291–296, https://doi.org/10.1007/s10549-020-05641-2.